Ankle Joint Torque Estimation Using an EMG-Driven Neuromusculoskeletal Model and an Artificial Neural Network Model

Longbin Zhang, Zhijun Li, *Senior Member, IEEE*, Yingbai Hu, Christian Smith, *Member, IEEE*, Elena M. Gutierrez Farewik, and Ruoli Wang

***Abstract*— In recent decades, there has been an increasing interest in the use of robotic powered exoskeletons to assist patients with movement disorders in rehabilitation and daily life. Providing assistive torque that compensates for the user's remaining muscle contributions is a growing and challenging field within exoskeleton control. In this article, ankle joint torques were estimated using electromyography (EMG)-driven neuromusculoskeletal (NMS) model and an artificial neural network (ANN) model in seven movement tasks, including fast walking, slow walking, self-selected speed walking, and isokinetic dorsi/plantar flexion at 60°/*s* and 90°/*s*. In each method, EMG signals and ankle joint angles were used as input, the models were trained with data from 3-D motion analysis, and ankle joint torques were predicted. Six cases using different motion trials as calibration (for the NMS model)/training (for the ANN) were devised, and the agreement between the predicted and measured ankle joint torques was computed. We found that the NMS model could overall better predict ankle joint torques from EMG and angle data than the ANN model with some exceptions; the ANN predicted ankle joint torques with better agreement when trained with data from the same movement. The NMS model predicted ankle joint torque best when calibrated with trials during which EMG reached maximum levels, whereas the ANN predicted well when trained with many trials and types of movements. In addition, the ANN prediction may become less reliable when predicting unseen movements. Detailed comparative studies of methods to predict ankle joint torque are crucial for determining strategies for exoskeleton control.**

***Note to Practitioners*—In exoskeleton control for strength augmentation applied in military, industry, and healthcare applications, providing assistive torque that compensates for the user's remaining muscle contributions, is a challenging problem. This article predicted the ankle joint torques by electromyography (EMG)-driven neuromusculoskeletal (NMS) model and an artificial neural network (ANN) model in different movements. To the best of our knowledge, this is the first study comparing joint torque prediction performance of EMG-driven model to ANN. In the EMG-driven NMS model, mathematical equations were formulated to reproduce the transformations from EMG signal generation and joint angles to musculotendon forces and joint torques. A three-layer ANN was constructed with an adaptive moment estimation (Adam) optimization method to learn the relationships between the inputs (EMG signals and joint angles) and the outputs (joint torques). In the experiments, we estimated ankle joint torques in gait and isokinetic movements and compared the performance of methods to predict ankle joint torque, relating to how the methods have been calibrated/trained. The detailed analysis of the methods' performance in predicting ankle joint torque can significantly contribute to determining which model to choose, and under which circumstances, and, thus, be of great benefit for exoskeleton rehabilitation controller design.**

***Index Terms*— Adaptive moment estimation (Adam), hill-type muscle model, musculotendon kinematics, OpenSim.**

Manuscript received June 17, 2020; accepted October 18, 2020. Date of publication November 16, 2020; date of current version April 7, 2021. This article was recommended for publication by Associate Editor C. Krishnan and Editor M. Zhang upon evaluation of the reviewers' comments. This work was supported in part by the Promobilia Foundation under Grant 18200 and Grant 18014 and in part by the Swedish Research Council under Grant 2018-00750 and Grant 2018-04902. The work of Longbin Zhang was supported by the China Scholarship Council (CSC). The work of Yingbai Hu was supported by the Zhejiang Lab's International Talent Fund for Young Professionals. *(Corresponding author: Ruoli Wang.)*

Longbin Zhang is with the KTH MoveAbility Lab, KTH BioMEx Center, Department of Engineering Mechanics, KTH Royal Institute of Technology, SE-100 44 Stockholm, Sweden (e-mail: longbin@kth.se).

Zhijun Li is with the Department of Automation, University of Science and Technology of China, Hefei 230060, China (e-mail: zjli@ieee.org).

Yingbai Hu is with the Department of Informatics, Technical University of Munich, 85748 Munich, Germany (e-mail: yingbai.hu@tum.de).

Christian Smith is with the Robotics Perception and Learning Lab, KTH Royal Institute of Technology, SE-100 44 Stockholm, Sweden (e-mail: ccs@kth.se).

Elena M. Gutierrez Farewik and Ruoli Wang are with the KTH MoveAbility Lab, KTH BioMEx Center, Department of Engineering Mechanics, KTH Royal Institute of Technology, SE-100 44 Stockholm, Sweden, and also with Department of Women's and Children's Health, Karolinska Institutet, SE-100 44 Stockholm, Sweden (e-mail: lanie@kth.se; ruoli@kth.se).

Color versions of one or more of the figures in this article are available online at https://ieeexplore.ieee.org.

Digital Object Identifier 10.1109/TASE.2020.3033664

I. Introduction

PHYSICAL changes as a result of neurological disorders, for example, muscle weakness, poor coordination, and loss of sensation, affect daily activities, such as locomotion in a large number of people [1]. The rehabilitation of locomotion has always been a key priority for patients with movement disorders [2]. Devices have been developed to restore motor function and facilitate locomotion rehabilitation in individuals with spinal cord injury (SCI) and stroke, for instance. One such device is a powered exoskeleton [3], [4]. During exoskeleton-assisted rehabilitation, patients' active participation is essential in facilitating neuromuscular recovery [5]. However, despite the development in mechatronics and bioelectricity, exoskeleton control methods that involve the active participation of neurologically affected patients are still few, which limits the possibilities of inducing activity-driven neuroplastic changes that are needed for recovery [6].

During exoskeleton-assisted rehabilitation training, many control algorithms have been designed to increase patients' muscle strength, brain plasticity, and movement enhancement [7]. Neuhaus *et al.* [8] presented a robotic orthosis "Mina" for assisting mobility using recorded angle trajectories from an able-bodied individual for people with paraplegia. Farris *et al.* [9] proposed a powered lower extremity orthosis, which could provide assistive torque in the sagittal plane at hip and knee joints in persons with SCI in gait, based on joint angle trajectories from an able-bodied subject. However, these control algorithms used reference trajectories that were predefined for the complete gait cycle. Predefined trajectories do not facilitate the body's natural movement, nor do they consider how human muscles coordinate. In addition, individual adaptation is very difficult since it is not possible to smoothly transfer movement trajectories from one gait pattern to another. Therefore, designing exoskeleton control algorithms that enable the user's intentions instead of reference trajectories is in great demand.

Designing exoskeleton control algorithms based on the user's intention requires accurate and robust decoding of motor function, for instance, by recording underlying neuromuscular activities, such as the brain, nerve, and muscle electromyography (EMG) signals from the central nervous system (CNS) [10]–[13]. EMG signals are relatively easy to acquire and process and provide essential information on human motion compared with brain and nerve signals. EMG signals are nonlinearly related to muscle force and joint torque [14]. A model is needed to relate muscle activation and joint torque, for example, neuromusculoskeletal (NMS) models with modified Hill-type muscle model have been employed extensively [15], [16]. EMG-based modeling has also been integrated into various human–machine control strategies for exoskeleton actuators. Yao *et al.* [5] proposed an adaptive admittance control scheme for an ankle exoskeleton by utilizing an EMG-driven musculoskeletal model and tested on eight able-bodied subjects. They were able to achieve compliant joint assistance according to the real-time stiffness estimation of the ankle joint. Durandau *et al.* [6] developed a patient-specific computational NMS model with EMG signals to control a lower limb exoskeleton that assisted patients with paresis, resulting in a reduction in muscle activation and required physiological torque to perform a motor task with an increased level of exoskeleton assistance. Ronsse *et al.* [17] introduced a real-time estimate of velocity and acceleration based on an able-bodied subject's joint position using adaptive oscillators that could be applied as an impedance-based walking assistance strategy. Karavas *et al.* [18] presented a novel teleimpedance controller for a knee exoskeleton that provided assistance to an able-bodied subject based on the user's intention and joint stiffness. There is an obvious value in expanding these studies to develop an exoskeleton controller based on patients' neuromuscular abilities, taking into account the complex dynamics that involve both biomechanical and neurophysiological aspects. Therefore, constructing an EMG-driven NMS model to predict the user's physiological torque is of great importance in designing exoskeleton control strategies.

In recent years, artificial neural network (ANN) technology has been widely applied in classification, prediction, identification, and optimization problems [19]–[22] and has demonstrated power in many domains of modern society, such as marketing, agriculture, and healthcare [23]. Traditional myoelectric control strategies of exoskeleton assistive strategies require carefully constructed and chosen features. For example, an EMG-driven NMS model consists of complex calibration procedures and requires constructing complex relationships among different variables, such as EMG signals, muscle geometries, motion data, and joint torque. Alternatively, the ANN model can extract features on multiple levels of representation and predict very complex functions with a composition of enough representation layers without explicit descriptions of the complex relationships between variables. ANN methods have been applied to estimate lower limb joint torque during a vertical jump [24], isokinetic knee contractions [25], and elbow flexion movements [26]. ANN is, thus, a possible alternative to using an EMG-driven NMS model to map EMG signals to joint torque.

The objective of this study was to estimate ankle joint torque using an EMG-driven NMS model and an ANN model simultaneously. The agreement between the predicted and measured joint torque using two methods was compared and analyzed. Our hypotheses were that the ANN model would have a better overall performance than the EMG-driven NMS model, particularly when trained on a large amount of data, but that an EMG-driven NMS might have a better agreement when calibrated and tested on movements involving the similar muscle contraction coordination.

II. Methods

A. Experimental Setup

Ten able-bodied adults (age: 26 $\pm$ 2.86 years; weight: 70.36 $\pm$ 11.49 kg; height: 175.06 $\pm$ 8.45 cm; and sex: 4F/6M) were recruited. All participants provided informed written consent. Collection of the data was accomplished at the Biomechanics and Motor Control (BMC) Laboratory, Swedish School of Sport and Health Sciences (GIH), Stockholm, Sweden, and the study was approved by the regional ethics committee, Karolinska Institutet, Stockholm. Surface EMG electrodes were placed on the soleus (SOL), tibialis anterior (TA), and gastrocnemius medialis (GM) muscles of the right leg based on European recommendations for surface EMG [27].

A 3-D motion capture system (Qualisys, Gothenburg, Sweden) was used to record the trajectories of the markers placed on the subjects according to a conventional marker set (Plug-in Gait/CGM1) protocol [28], [29]. The experiments include gait analysis and ankle isokinetic dorsi/plantar flexion tests. The experiment setup is shown in Fig. 1. The subject was asked to first walk at a self-selected speed and then to synchronize steps to a metronome at 120 cadences/min and 100 cadences/min each for three times. Ground reaction forces (GRFs) were measured by two force plates (Kistler, Winterthur, Switzerland).

During isokinetic ankle movements, the subjects lay in a prone position with their right knee flexed at 20° and right

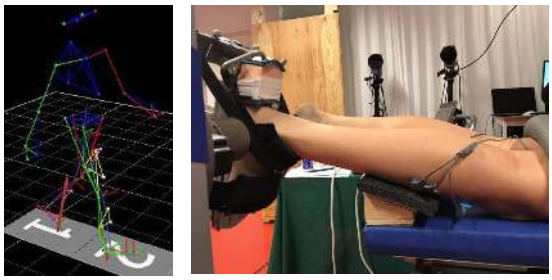

Fig. 1. Experimental setup. (a) Gait. (b) Isokinetic dorsi/plantar flexion movements.

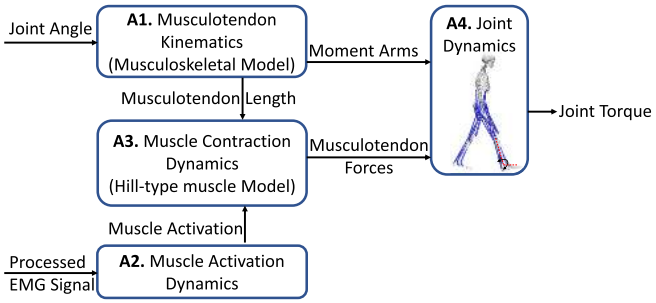

Fig. 2. Schematic of an EMG-driven NMS model. It consists of four components: A1—the model's musculotendon kinematics were used to calculate musculotendon lengths and moment arms; A2—muscle activation dynamics were employed to calculate the level of muscle activation involved in the processed EMG signals; A3—muscle contraction dynamics according to a Hill-type muscle model were applied to predict musculotendon force using the calculated musculotendon length and muscle activation as inputs; and A4—joint dynamics was used to compute joint torques using the calculated musculotendon forces and moment arms as inputs.

foot fixed to a footplate attached to an isokinetic dynamometer (IsoMed 2000, D & R GmbH, Hemau, Germany). The ankle joint angle and torque were recorded simultaneously. Each subject was encouraged to plantarflex with maximal effort, while the ankle was plantarflexed, and likewise, while the ankle was dorsiflexed, five consecutive times at a velocity of 60 and 90°/s within a range of motion of −20° plantarflexion and 15° dorsiflexion.

B. Data Processing

1) Gait: Marker trajectories were captured at 200 Hz, and GRFs were recorded at 3000 Hz. GRFs were low-pass filtered, and filtering was only applied to nonzero values. EMG signals were recorded at 3000 Hz, then high-pass filtered (20–500 Hz), rectified and low-pass filtered (6 Hz), and normalized to the maximum processed EMG value recorded across all trials [30]–[32]. Marker trajectories, GRFs, and EMG Data processing were performed in MOtoNMS toolbox [33], which processes experimental data, including marker trajectories, GRFs, and EMG Data, from C3D files in different motion capture systems and produces input data for NMS modeling software, for instance, OpenSim (SimTK, Stanford, USA). Joint angles and torques were computed in an open-source musculoskeletal modeling software (OpenSim 3.3). A generic musculoskeletal model (OpenSim gait 2354) was scaled using marker trajectories to fit each individual's anthropometry. The scaled model was then used to reconstruct the 3-D joint angles and torques in terms of the marker trajectories and GRFs captured during dynamic movements by solving inverse kinematics and inverse dynamics [30]. Inverse kinematics solves a weighted least square problem to minimize the distance between experimental $x_i^{\exp}$ and corresponding marker on the model x_i, as follows [34]:

$$\min_q \left(\sum_i^N \theta_i \| x_i^{\exp} - x_i \|^2 \right) \tag{1}$$

where q is generalized coordinates of the model and θ_i is the weights of the ith marker.

Inverse dynamics calculate the forces and torques of joints by solving dynamic equation of motion, as follows [35]:

$$M(q)\ddot{q} + C(q, \dot{q}) + G(q) = \tau \tag{2}$$

where $q, \dot{q}$, and $\ddot{q}$ are the position, velocity, and acceleration of the generalized coordinates. $M(q)$ is mass matrix, $C(q, \dot{q})$ is the centripetal and Coriolis forces matrix, $G(q)$ is the gravitational forces matrix, and τ is the vector of unknown generalized forces.

2) Isokinetic Ankle Dorsi/Plantarflexion: The ankle joint angle and torque were recorded at 5000 Hz during ankle isokinetic dorsi/plantarflexion tasks and then filtered with a fourth-order Butterworth low-pass filter with a cutoff frequency of 6 Hz. The EMG signals were processed in the same way as in gait. Ankle joint angles, torques, and EMG data were processed in MATLAB (MatlabR2017a, MathWorks Inc., Natick, MA, USA).

C. EMG-Driven Neuromusculoskeletal Model

A previously developed EMG-driven NMS model [15] was used in this study. It reproduces the transformations from EMG signal generation and joint angles to musculotendon forces and joint torques. The EMG-driven NMS model consists of four components: musculotendon kinematics, muscle contraction dynamics, muscle activation dynamics, and joint dynamics [36] (see Fig. 2).

The musculotendon kinematics component used the 3-D joint angles to calculate musculotendon lengths and moment arms of individual musculotendon units (MTUs) through a musculoskeletal model. The muscle activation dynamics component calculated muscle activation based on filtered EMG signals. The relation between neural activation $u(t)$ and filtered EMG signal $e(t)$ was represented by a recursive filter [37] as follows:

$$u_i(t) = \alpha e_i(t-d) - \beta_1 u_i(t-1) - \beta_2 u_i(t-2) \tag{3}$$

where $e_i(t)$ is the linear envelope of the EMG signal of the ith muscle; $u_i(t)$ is the neural activation of the ith muscle; d is the electromechanical delay; α is the muscle gain coefficient; and β_1 and β_2 are the recursive coefficients and are subject to the following constraints to obtain a stable solution [15], [37], [38]: $\beta_1 = C_1 + C_2$ and $\beta_2 = C_1 \cdot C_2$, where $|C_1| < 1$, $|C_2| < 1$, and $\alpha - \beta_1 - \beta_2 = 1$

A nonlinear relationship from neural activation to muscle activation was formulated to describe muscle activation dynamics as follows:

$$a_i(t) = \frac{e^{A_i u_i(t)} - 1}{e^{A_i} - 1} \tag{4}$$

where $a_i(t)$ is the ith muscle activation; A_i is the nonlinear shape factor of ith muscle and subjected to the interval $(-3, 0)$, with zero representing a linear relationship, and negative values introduce a nonlinear relationship between neural activation and muscle activation [32], [38].

Musculotendon forces were computed through muscle contraction dynamics based on a three-element Hill-type muscle model: a series elastic element (SE), a contractile element (CE), and a parallel elastic element (PE). Each MTU's force (F^{mt}) could be represented as a function of muscle activation and muscle kinematics as follows:

$$F^{mt} = F_0^m \left[f_a\left(\tilde{l}_m\right) \cdot f_v(\tilde{v}_m) \cdot a + f_p\left(\tilde{l}_m\right) + d_m \tilde{v}_m \right] \cos(\phi) \tag{5}$$

where F_0^m is the maximum isometric muscle force; $f_a(\tilde{l}_m)$ is the active force–length relationship that describes the ability of muscle fibers to generate forces at different lengths; $\tilde{l}_m$ is the fiber length normalized with the optimal fiber length; $f_v(\tilde{v}_m)$ is the force–velocity relationship that represents the muscle fiber force contribution of the fibres' contraction velocity ($\tilde{v}_m$), and the velocity was normalized with maximum contraction velocity and optimal fiber length; $f_p(\tilde{l}_m)$ is the passive force–length relationship that expresses the force response to the fibers to strain; d_m is the muscle damping coefficient that represents the muscle damping characteristics; and ϕ is the pennation angle of the fibers.

Joint torques were then estimated by the product of musculotendon forces F_{mt} and moment arms r_{mt} through the joint dynamics component as follows:

$$M = r_{mt} \times F^{mt}. \tag{6}$$

The EMG-driven NMS model was implemented in OpenSim through the calibrated EMG-informed NMS modeling toolbox (CEINMS) [15]. OpenSim was also used to calculate musculotendon lengths and moment arms using joint angles through the scaled musculoskeletal model [39]. CEINMS was then employed to calibrate a subject-specific EMG-driven NMS model to predict joint torques.

Detailed parameter configuration of the EMG-driven NMS model followed the recommendation by Pizzolato *et al.* [15]. For each subject-specific EMG-driven NMS model, optimal fiber of length l_0^m and tendon slack of length l_s^t of each MTU were bounded within $\pm 15\%$ from their initial values, and muscle activation dynamics parameters A, C_1, and C_2 were calibrated globally. The shape factor A was bounded between -3 and 0, and the coefficients C_1 and C_2 were bounded between -1 and 1. A strength coefficient constrained between 0.5 and 2.5 was assigned to each MTU and was used to calibrate maximum isometric force. During the calibration, these subject-specific parameters were refined by an optimization algorithm to minimize the error between estimated and measured/actual ankle joint torques.

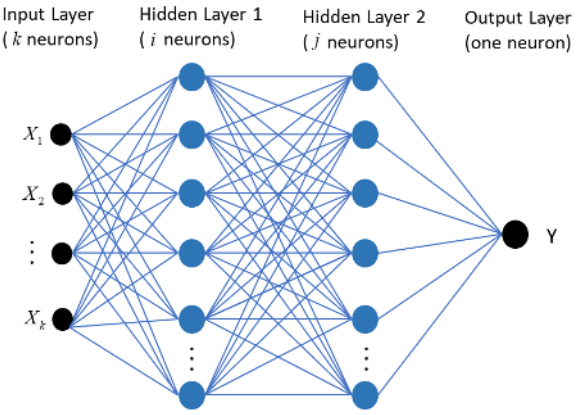

Fig. 3. Three-layer ANN architecture with k input neurons ($k = 4$, including EMG recordings from three muscles and ankle joint angle), two hidden layers with i and j neurons, respectively ($i = 10$ and $j = 10$), and one output neuron of the predicted ankle joint torque Y.

D. Artificial Neural Network Model

The ANN model that was used to estimate ankle joint torque consists of an input neural layer (experimentally measured data as the input variables), an output neural layer (where the predicted ankle joint torque was determined), and two hidden layers (where the convergence work of the neural network was facilitated).

At the input layer (see Fig. 3), each neuron represented input variables $(X_1, \ldots, X_k)$, including EMG recordings and ankle angle ($k = 4$). The input variables spread to the hidden layer by the propagation rule as follows:

$$S_i = \sum_{k=1}^{N} W_{ki} X_k + b_i \tag{7}$$

where S_i is the ith output in the first hidden layer ($i = 10$), W_{ki} is the weight value of the connection between neurons k from the input layer and neurons i from the first hidden layer, and b_i is the value of the bias value associated with neuron i. For the second hidden layer with j neurons ($j = 10$), output from the previous layer output was set as input and spread to the next layer.

Each neuron in the hidden layer used a rectifier linear unit (ReLU) $S_i = \max(S_i, 0)$ as its activation function. In practice, training of a ReLU network outperformed other activation functions, such as sigmoid and tanh, with respect to the statistical performance and the computational cost [40], [41]. The output layer that predicted ankle joint torque is a linear combination of weighted hidden layer outputs with biases of the ANN.

In the training process of the ANN model, a mean square error (mse) between the predicted and measured ankle joint torque was used as the loss function L, as shown in the following equation:

$$L = 1/n \sum_{i=1}^{n} \left(y_{i,\text{predict}} - y_{i,\text{measure}} \right) \tag{8}$$

where n is the number of data samples; y_{predict} and y_{measure} are the predicted and measured ankle joint torque, respectively.

The trained ANN aimed to achieve a globally optimal solution by using an adaptive moment estimation (Adam) optimization method. The Adam was proposed by Kingma and Ba [42] and is currently one of the most popular step size methods in the area of ANNs [43]. Adam adjusts the learning rate automatically for each weight based upon the first and second moments of the gradients (the mean and uncentered variance) for that weight.

To train an eligible ANN model with a low loss [computed from (8)], a "coarse-to-fine" random search was utilized to obtain the parameters included in the model. Two hidden fully connected layers with ten neurons were applied, and the ReLU activation function was used. The learning rate of the Adam optimizer was tuned to 0.0009. The batch size of the ANN was set to 20. A Xavier weight with zero bias initializer was chosen, and 500 epochs were used.

E. Evaluation Protocol

To investigate and compare the efficiency and accuracy of predicting ankle torque through the EMG-driven NMS model and the ANN, six different cases were formed, using different types of trials to calibrate (NMS model) or train (ANN) the model. After calibrating (training), the parameters for the NMS model were obtained, including optimal fiber length and tendon slack length of each MTU, muscle activation dynamics parameters, and maximum isometric force; the parameters for the ANN model were also acquired, including hidden layer neurons, learning rate, batch size, initializer, and the number of epochs. The calibrated and trained models were each then tested on the remaining trials. The six different cases were chosen to validate the proposed hypotheses that the ANN model would have a better overall performance than the EMG-driven NMS model, but an EMG-driven NMS might have a better agreement when calibrated and tested on movements involving the same muscle contractions. Calibration/training data are as follows.

- *Case 1:* Three trials from slow walking at 100 cadences/min.
- *Case 2:* Three trials from isokinetic plantarflexion at 90°/s.
- *Case 3:* Three trials from dorsiflexion at 90°/s.
- *Case 4:* Three trials from dorsiflexion at 60°/s and three trials from plantarflexion at 60°/s.
- *Case 5:* Two trials from (each) slow walking at 100 cadences/min, self-selected walking speed, dorsiflexion at 60°/s, dorsiflexion at 90°/s, plantarflexion at 60°/s, and plantarflexion at 90°/s, separately.
- *Case 6:* Three trials that included maximum signal processed EMG magnitudes across all trials of the SOL, GM, and TA muscles.

The root mse (RMSE) E_{rms} between the measured (computed from inverse dynamics) and predicted ankle joint torque (normalized by body mass) is used to evaluate the agreement of each model. RMSE was computed for each subject and then averaged across the ten subjects

$$E_{\text{rms}} = \sqrt{1/N \sum_{i=1}^{n} \left(y_p - y_a\right)} \tag{9}$$

where y_p and y_a are the predicted and actual ankle joint torques, respectively. A paired t-test was applied to investigate the agreement between the measured and predicted joint torques by the NMS model and ANN (at 5% level of significance).

III. Results

In Case 1, the predicted torque from both the NMS model and the ANN agreed better with measured torque in gait than in the isokinetic ankle movements, among which agreement was somewhat better in the plantarflexor movement. Compared with NMS, the ANN-predicted torque agreement was found significantly better in calibrated/trained slow walking movement ($p < 0.01$). No significant differences were found between two methods in other movements (see Fig. 4). The mean and SD of RMSE across ten subjects were shown Table I.

In Case 2, torques predicted by both the NMS model and the ANN agreed better with measured torques in plantarflexion movements than in gait and dorsiflexion movements, with the poorest agreement in dorsiflexion movements. Compared with NMS, the ANN-predicted torque agreement was significantly better in plantarflexion tasks ($p = 0.01$ and $p = 0.03$) but significantly worse in gait ($p = 0.05$, $p = 0.01$, and $p = 0.04$). Although the RMSE of torque prediction was lower in NMS model in dorsiflexion tasks, the differences were not significant ($p = 0.15$ and $p = 0.10$).

In Case 3, torques predicted by both the NMS model and the ANN agreed better with measured torques in dorsiflexion movements than in gait and plantarflexion movements. Compared with NMS, the ANN-predicted torque agreement was significantly better in dorsiflexion tasks ($p < 0.01$) but significantly worse in gait ($p = 0.02$, $p = 0.01$, and $p < 0.01$). Although the RMSE of torque prediction was lower in the NMS model in plantarflexion tasks, the differences were not significant ($p = 0.11$ and $p = 0.07$). In total, the RMSE of torque prediction from the NMS model was significantly lower than in ANN ($p = 0.03$).

In Case 4, torques predicted by both the NMS model and the ANN agreed better in dorsiflexion and plantarflexion movements than in gait. Compared with NMS, the ANN-predicted torque agreement was significantly better in the calibrated/trained plantarflexion and dorsiflexion movements ($p < 0.01$). Although the RMSE of torque prediction was lower in NMS model in gait, the differences were not significant ($p = 0.44$, $p = 0.63$, and $p = 0.33$).

In Case 5, compared with the first four cases, predicted torques by both the NMS model and the ANN agreed better overall. The ANN-predicted torque agreement was better than NMS-predicted torque in all movements. The overall RMSE of torque prediction was significantly lower in ANN than in the NMS model. There was a significant difference between the RMSEs estimated by the NMS model and ANN in gait ($p < 0.01$) and 90 °/s plantarflexion ($p = 0.03$) and 90 °/s dorsiflexion ($p < 0.01$) movements. Although the RMSE of torque prediction was lower in the ANN model in 60 °/s dorsiflexion and 60 °/s dorsiflexion movements, the differences were not significant ($p = 0.05$ and $p = 0.37$).

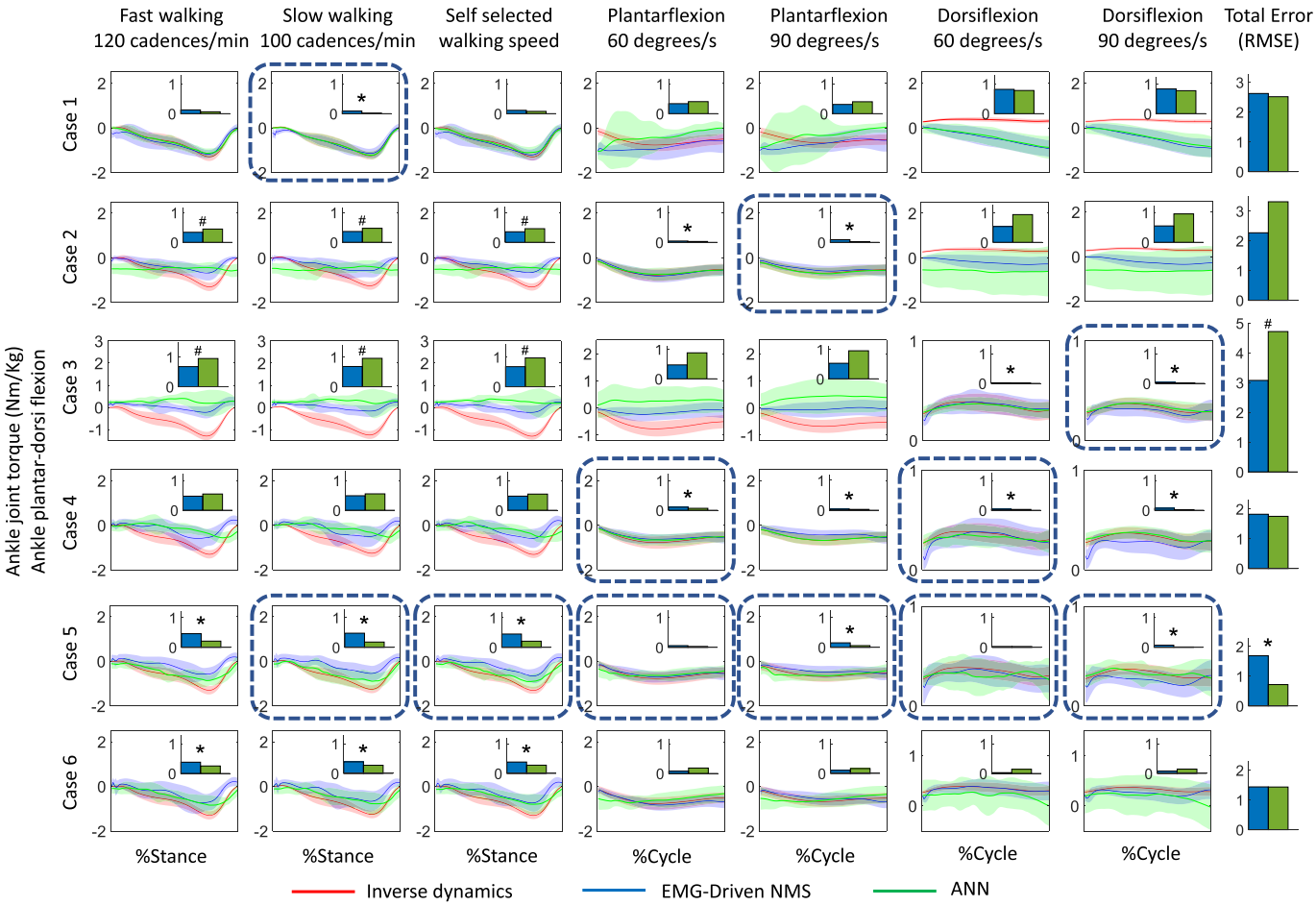

Fig. 4. Ankle joint torque estimated via inverse dynamics, EMG-driven NMS model, and ANN, shown as mean ± 1 standard deviation (SD) of all subjects and trials. Results of gait are shown during the stance phase. The isokinetic dorsi/plantarflexion movements are shown as a function of the movement cycle. Six different cases using different types of trials for calibration (NMS) or training (ANN), tested on the remaining trials, were created. The trials used for calibration/training trials are circled. Case 1: three trials from slow walking at 100 cadences/min. Case 2: three trials from plantarflexion at 90 °/s. Case 3: three trials from dorsiflexion at 90 °/s. Case 4: three trials from dorsiflexion at 60 °/s and three trials from plantarflexion at 60 °/s. Case 5: two trials from slow walking at 100 cadences/min, self-selected walking speed, dorsiflexion at 60 °/s, dorsiflexion at 90 °/s, plantarflexion at 60 °/s, and plantarflexion at 90 °/s, separately. Case 6: three trials containing the maximum EMG value from all trials of the SOL, GM, and TA muscles. The agreement of predicted ankle torque (normalized by body mass) from each model with the observed value (inverse dynamics) was computed as the RMSE. The RMSE was calculated for each subject, and an average was computed, as illustrated in the column plots. ∗ and # indicate that the RMSE estimated by ANN was significantly lower and higher than the NMS model, respectively, based on a paired t-test.

In Case 6, compared with the results in Case 5, predicted torques by the NMS model agreed better with measured torques, whereas those predicted by the ANN were somewhat worse. There was a significant difference between the RMSEs predicted by the NMS model and ANN in gait ($p = 0.02$, $p = 0.02$, and $p = 0.04$). No significant differences were found between the two methods in other movements.

IV. Discussion

We estimated the ankle joint torques using two relevant, but fundamentally different methods: an EMG-driven NMS model and an ANN. This article is the first study comparing joint torque prediction performance of an EMG-driven NMS model to ANN in different movements, using different training data as input. We found that the NMS model had a better agreement in ankle joint torque prediction than the ANN model with some exceptions; the ANN predicted ankle joint torques with better agreement when trained with data from the same movement type. The NMS model predicted ankle joint torque best when calibrated with trials during which EMG reached maximum levels, whereas the ANN predicted well when trained with many trials and types of movements. In this article, the detailed comparative performance of methods to predict ankle joint torque, relating to how the methods have been calibrated/trained, can significantly contribute to deciding which model to choose in which circumstances and, thus, be of large benefit for exoskeleton rehabilitation controller design.

Both the EMG-driven NMS and ANN model-based methods have been commonly applied in limb joint torque estimation, but their respective advantages in prediction were not well investigated. Ankle joint torques and joint stiffness predicted by an EMG-driven NMS model were used as the inputs of an ankle exoskeleton controller [5]; a significant correlation was reported between the predicted and measured ankle joint stiffness, as well as torque, respectively. Meyer *et al.* [44] proposed an EMG-driven modeling approach that can automatically

TABLE I
MEAN AND SD OF RMSE ACROSS TEN SUBJECTS IN ANKLE JOINT TORQUE ESTIMATION

Training/	Fast walking		slow walking		Self-selected		Plantaflexion		Plantaflexion		Dorsiflexion		Dorsiflexion			
Calibration	120 cadences/min		100 cadences/min		walking speed		60 degrees/s		90 degrees/s		60 degrees/s		90 degrees/s		Total Error	
Model	EMG-driven	ANN	EMG-driven	ANN	EMG-driven	ANN	EMG-driven	ANN	EMG-driven	ANN	EMG-driven	ANN	EMG-driven	ANN	EMG-driven	ANN
Case 1 RMSE (SD)	0.13 (0.13)	0.06 (0.03)	**0.09 (0.06)**	**0.01 (0.01)**	0.11 (0.11)	0.08 (0.06)	0.34 (0.30)	0.40 (0.54)	0.31 (0.19)	0.40 (0.70)	0.82 (0.32)	0.78 (0.31)	0.83 (0.32)	0.77 (0.35)	2.62 (1.15)	2.51 (1.02)
Case 2 RMSE (SD)	**0.34 (0.13)**	**0.45 (0.14)**	**0.36 (0.17)**	**0.47 (0.15)**	**0.36 (0.16)**	**0.46 (0.15)**	**0.04 (0.05)**	**0.03 (0.03)**	**0.09 (0.05)**	**0.02 (0.03)**	0.53 (0.26)	0.93 (0.95)	0.55 (0.25)	0.95 (0.94)	2.27 (0.32)	3.31 (2.11)
Case 3 RMSE (SD)	**0.68 (0.18)**	**0.95 (0.30)**	**0.68 (0.17)**	**0.96 (0.30)**	**0.67 (0.20)**	**0.97 (0.30)**	0.47 (0.26)	0.87 (0.59)	0.52 (0.26)	0.94 (0.62)	**0.02 (0.02)**	**0.02 (0.01)**	**0.03 (0.01)**	**0.01 (0.01)**	**3.07 (0.83)**	**4.72 (1.79)**
Case 4 mean (SD)	0.47 (0.09)	0.54 (0.09)	0.49 (0.12)	0.55 (0.15)	0.47 (0.12)	0.54 (0.10)	**0.10 (0.08)**	**0.06 (0.04)**	**0.18 (0.10)**	**0.01 (0.03)**	**0.04 (0.03)**	**0.03 (0.02)**	**0.08 (0.04)**	**0.01 (0.01)**	1.82 (0.35)	1.75 (0.31)
Case 5 RMSE (SD)	**0.46 (0.05)**	**0.21 (0.10)**	**0.47 (0.11)**	**0.18 (0.09)**	**0.45 (0.08)**	**0.20 (0.10)**	0.06 (0.07)	0.03 (0.03)	**0.15 (0.11)**	**0.06 (0.04)**	0.03 (0.04)	0.03 (0.03)	**0.07 (0.04)**	**0.01 (0.01)**	**1.67 (0.21)**	**0.71 (0.25)**
Case 6 RMSE (SD)	**0.38 (0.15)**	**0.25 (0.25)**	**0.39 (0.15)**	**0.27 (0.26)**	**0.38 (0.15)**	**0.28 (0.27)**	0.08 (0.21)	0.18 (0.20)	0.10 (0.15)	0.16 (0.20)	0.03 (0.03)	0.14 (0.21)	0.08 (0.05)	0.15 (0.28)	1.44 (0.26)	1.43 (0.46)

modify surrogate representations of the user's musculoskeletal geometry and improve the accuracy of lower limb joint torques prediction in gait. The EMG-driven NMS model uses mathematical equations to reproduce the transformations from EMG signal generation and joint angles to musculotendon forces and joint torques. Subject-specified EMG-driven model calibrated with personalized musculoskeletal geometry, such as moment arms and muscle characteristics, could improve its reliability in joint torque prediction. However, the EMG-driven NMS model consists of complex calibration procedures and requires the construction of complex relationships among different variables, such as EMG signals, muscle geometries, motion data, and joint torque. Alternatively, ANN can extract features and store information on the entire network and predict very complex functions, with a composition of enough representation layers without explicit descriptions of the complex relationships between variables. Hahn [25] used a three-layer ANN model to estimate knee torques in 30 and 60 °/s isokinetic extension/flexion, and their results showed that the ANN model had a more accurate torque prediction compared with the stepwise regression model. Jali *et al.* [26] applied a three-layer ANN to estimate joint torque during elbow flexion movements. Their results illustrated that ANN could well-demonstrate the EMG-torque relation and could be utilized in the torque control in arm rehabilitation devices. Liu *et al.* [24] used a three-layer ANN to estimate lower limb joint torques during a vertical jump using GRF data as inputs, and their study revealed that ANN could estimate the nonlinear relation between GRF data and lower limb joint torques during a vertical jump. However, ANN could be used to map the relations between inputs and outputs, but it does not explain the behavior of the network and, thus, reduces its reliability in the network. There are both advantages and disadvantages in the EMG-driven NMS model and the ANN model; however, a comparison between ankle torques predicted by an EMG-driven NMS and an ANN model has not been performed.

The ANN prediction performed well when trained on data from similar movements but might become less reliable when predicting unseen movements. In Cases 1–4, a lower RMSE from ANN was found in the gait, plantarflexion, dorsiflexion, and dorsi/plantar flexion tasks, respectively, compared with the EMG-driven NMS model when the same motions were included in calibration/training the model. Particularly, in Case 5, a lower RMSE was found in all tasks in the ANN model, and the overall RMSE from ANN was significantly lower than the NMS model when all types of movements were included in the training process. In the ANN model, a three-layer neural network with two hidden layers was constructed. The input variables spread data features to hidden layers. Two hidden layers were commonly chosen and stated to be sufficient to express most of the relations in society [45]. More hidden layers would construct a more complex neural network than needed and likely cause overfitting [46]. The data amount in this study might not be large enough to build a complex neural network with more hidden layers. The neurons in hidden layers learn a different set of weights and biases to represent different functions over the input data. The ReLu activation function was applied independently to each element of the hidden layer to add a nonlinear property to the neural network and, thus, learn more complex relationships and patterns in the data. The Adam optimization method trained the ANN model to achieve a globally optimal solution, while other parameters were chosen by "coarse-to-fine" random search based on trial and error to have a lower loss when training the ANN model. With the similar movements' data, the constructed ANN model could extract the complex nonlinear relationship between EMG signals and joint torque and, thus, has a better agreement in torque prediction in similar movements compared with the NMS model. Therefore, ANN is superior to the NMS model in estimating the limb joint torque in the same types of movement as in the training process. However, the ANN prediction might become less reliable when encountering unseen movements.

For example, ANN-predicted torque agreement was worse and had a larger SD in isokinetic plantarflexion in Cases 1 and 3 and dorsiflexion in Cases 2 and 6 than in the NMS model when the movements were not included in the training process. This could be explained that ANN learns the relationships between inputs and outputs with training movements' data as a black box, resulting in the unexplained behavior of the network. The trained ANN model probably did not learn the relations between variables in unseen tasks and became unpredictable; thus, they have a worse prediction agreement. Therefore, the overall RMSE might have been lower at times, but the larger variability probably makes it less reliable when encountering unseen movements.

It is important to note that the ANN model only learns the relationships between inputs (EMG signals and ankle angle) and output (ankle torque) through its hidden layers; no other relevant information about muscle or joint contact forces, for example, is explicitly computed. It is, thus, only suitable to predict the specifically designated outputs. The NMS model, in contrast, has intermediate steps in which relevant information is computed and can be useful in other contexts. Computed muscle forces, for instance, are computed in intermediate steps and could be used to compute joint stiffness and as input for an ankle exoskeleton controller, for instance, as seen in the work by Yao *et al.* [5].

Trained EMG-driven NMS model, however, overall predicted ankle torques better than the ANN, in movements that have similar muscle contraction as in the calibration movements. For instance, in Case 2, the EMG-driven NMS predicted joint torques were significantly better in gait and in isokinetic plantarflexion than in isokinetic dorsiflexion. This can be attributed to the observation that, in gait and isokinetic plantarflexion, SOL and GM both worked as dominant muscles for movements and possibly have similar muscle coordination patterns. In the EMG-driven NMS model, muscle coordination in terms of relative timing and relative magnitude [47], [48] were explicitly taken into account during the calibration procedure, so, if the unseen movements have similar muscle coordination patterns, the EMG-driven NMS model will work better. Therefore, the EMG-driven model had a better performance in predicting limb joint torque of unseen tasks that involve similar muscle contraction coordination as in the calibration task.

Calibrating on a large number of trials did not in general improve the performance of the NMS in predicting joint torques but did improve the performance of the ANN. The overall RMSE of ANN-predicted torques in Case 5 was significantly lower than those of NMS-predicted torques. The ANN model utilized self-selected neurons and neural network layers to estimate the nonlinear relationships between input signals and regression outputs. With a large amount of data, ANN could learn more essential properties associated with the relationships between EMG signals and joint torques. In contrast, the NMS-predicted torques agreed with measured torques best in Case 6. In the EMG-driven NMS model, mathematical equations were formulated to represent the nonlinear relationships between EMG signals and torques, and optimization algorithms were used to calibrate other MTU-specific parameters, such as optimal fiber length and maximum isometric force. With high EMG magnitude, a large range of muscle force–length, force–velocity, and tendon force–strain relationships are included in the calibration process and, thus, well-calibrate MTU-related parameters. As such, the calibration was more reliable when performed on trials containing relatively high EMG magnitude.

It is important to note that we only tested only one ANN and one NMS model. Other NMS models and even different parameters in the currently used NMS may have shown different results. There are likewise many other ANNs and machine learning models that have different structures and would likely have yielded different results. Our findings should be considered in this context. Another limitation of this study was that only ankle joint torque prediction performance using the two methods was compared. Only TA, GA, and SOL EMG signals and ankle joint angles were available. Knee and hip joint torque can be predicted, and comparative results could be more informative and robust if EMG data of more lower limb muscles were recorded in more different movements.

V. Conclusion

In this article, we presented detailed comparisons of ankle joint torque prediction between an EMG-driven NMS model and an ANN. In our study protocol, the EMG-driven NMS model better predicted joint torque from EMG and joint angle data with some exceptions; the NMS predicted ankle torques better when calibrated on trials involving a high degree of muscle activation, whereas the ANN predicted ankle torques somewhat better when trained on a large and varied set of trials. The detailed analysis of the methods' performance in predicting ankle joint torque can significantly contribute to determining which model to choose, and under which circumstances, and, thus, be of large benefit for exoskeleton rehabilitation controller design. As there are other NMS models and very many other machine learning algorithms, further investigation with other NMS models and machine learning algorithms are warranted to determine which approach is preferable to predict joint torque in different situations.

References

[1] A. Pedrinelli, L. E. Garcez-Leme, and R. D. S. A. Nobre, "The effect of physical training on the locomotor apparatus in elderly people," *Revista Brasileira de Ortopedia*, vol. 44, no. 2, pp. 96–101, Jan. 2009.

[2] Z. Liu, B. Zhong, W. Zhong, K. Guo, and M. Zhang, "A new trajectory determination method for robot-assisted ankle ligament rehabilitation," in *Proc. 41st Annu. Int. Conf. IEEE Eng. Med. Biol. Soc. (EMBC)*, Jul. 2019, pp. 5390–5393.

[3] R. A. R. C. Gopura, D. S. V. Bandara, K. Kiguchi, and G. K. I. Mann, "Developments in hardware systems of active upper-limb exoskeleton robots: A review," *Robot. Auto. Syst.*, vol. 75, pp. 203–220, Jan. 2016.

[4] M. Zhang, A. McDaid, A. J. Veale, Y. Peng, and S. Q. Xie, "Adaptive trajectory tracking control of a parallel ankle rehabilitation robot with joint-space force distribution," *IEEE Access*, vol. 7, pp. 85812–85820, 2019.

[5] S. Yao, Y. Zhuang, Z. Li, and R. Song, "Adaptive admittance control for an ankle exoskeleton using an EMG-driven musculoskeletal model," *Frontiers Neurorobotics*, vol. 12, p. 16, Apr. 2018.

[6] G. Durandau *et al.*, "Voluntary control of wearable robotic exoskeletons by patients with paresis via neuromechanical modeling," *J. NeuroEngineering Rehabil.*, vol. 16, no. 1, p. 91, Dec. 2019.

[7] K. Fujii *et al.*, "The voluntary driven exoskeleton hybrid assistive limb (HAL) for postoperative training of thoracic ossification of the posterior longitudinal ligament: A case report," *J. Spinal Cord Med.*, vol. 40, no. 3, pp. 361–367, May 2017.

[8] P. D. Neuhaus, J. H. Noorden, T. J. Craig, T. Torres, J. Kirschbaum, and J. E. Pratt, "Design and evaluation of mina: A robotic orthosis for paraplegics," in *Proc. IEEE Int. Conf. Rehabil. Robot.*, Jun. 2011, pp. 1–8.

[9] R. J. Farris, H. A. Quintero, and M. Goldfarb, "Preliminary evaluation of a powered lower limb orthosis to aid walking in paraplegic individuals," *IEEE Trans. Neural Syst. Rehabil. Eng.*, vol. 19, no. 6, pp. 652–659, Dec. 2011.

[10] M. Sartori, G. Durandau, S. Došen, and D. Farina, "Robust simultaneous myoelectric control of multiple degrees of freedom in wrist-hand prostheses by real-time neuromusculoskeletal modeling," *J. Neural Eng.*, vol. 15, no. 6, Dec. 2018, Art. no. 066026.

[11] M. Zhang, W. Meng, T. C. Davies, Y. Zhang, and S. Q. Xie, "A robot-driven computational model for estimating passive ankle torque with subject-specific adaptation," *IEEE Trans. Biomed. Eng.*, vol. 63, no. 4, pp. 814–821, Aug. 2015.

[12] Z. Li *et al.*, "Hybrid brain/muscle signals powered wearable walking exoskeleton enhancing motor ability in climbing stairs activity," *IEEE Trans. Med. Robot. Bionics*, vol. 1, no. 4, pp. 218–227, Nov. 2019.

[13] Z. Li, J. Li, S. Zhao, Y. Yuan, Y. Kang, and C. L. P. Chen, "Adaptive neural control of a kinematically redundant exoskeleton robot using brain–machine interfaces," *IEEE Trans. Neural Netw. Learn. Syst.*, vol. 30, no. 12, pp. 3558–3571, Dec. 2019.

[14] E. Trigili *et al.*, "Detection of movement onset using EMG signals for upper-limb exoskeletons in reaching tasks," *J. NeuroEngineering Rehabil.*, vol. 16, no. 1, p. 45, Dec. 2019.

[15] C. Pizzolato *et al.*, "CEINMS: A toolbox to investigate the influence of different neural control solutions on the prediction of muscle excitation and joint moments during dynamic motor tasks," *J. Biomechanics*, vol. 48, no. 14, pp. 3929–3936, Nov. 2015.

[16] A. Erdemir, S. McLean, W. Herzog, and A. J. van den Bogert, "Model-based estimation of muscle forces exerted during movements," *Clin. Biomechanics*, vol. 22, no. 2, pp. 131–154, Feb. 2007.

[17] R. Ronsse *et al.*, "Real-time estimate of period derivatives using adaptive oscillators: Application to impedance-based walking assistance," in *Proc. IEEE/RSJ Int. Conf. Intell. Robots Syst.*, Oct. 2012, pp. 3362–3368.

[18] N. Karavas, A. Ajoudani, N. Tsagarakis, J. Saglia, A. Bicchi, and D. Caldwell, "Tele-impedance based stiffness and motion augmentation for a knee exoskeleton device," in *Proc. IEEE Int. Conf. Robot. Autom.*, May 2013, pp. 2194–2200.

[19] G. Chen, H. Cao, J. Conradt, H. Tang, F. Rohrbein, and A. Knoll, "Event-based neuromorphic vision for autonomous driving: A paradigm shift for bio-inspired visual sensing and perception," *IEEE Signal Process. Mag.*, vol. 37, no. 4, pp. 34–49, Jul. 2020.

[20] L. Zhang, Z. Li, and C. Yang, "Adaptive neural network based variable stiffness control of uncertain robotic systems using disturbance observer," *IEEE Trans. Ind. Electron.*, vol. 64, no. 3, pp. 2236–2245, Mar. 2017.

[21] Z. E. Kanat and N. Özdil, "Application of artificial neural network (ANN) for the prediction of thermal resistance of knitted fabrics at different moisture content," *J. Textile Inst.*, vol. 109, no. 9, pp. 1247–1253, Sep. 2018.

[22] Y. Hu, X. Wu, P. Geng, and Z. Li, "Evolution strategies learning with variable impedance control for grasping under uncertainty," *IEEE Trans. Ind. Electron.*, vol. 66, no. 10, pp. 7788–7799, Oct. 2019.

[23] H. Su, Y. Hu, H. R. Karimi, A. Knoll, G. Ferrigno, and E. De Momi, "Improved recurrent neural network-based manipulator control with remote center of motion constraints: Experimental results," *Neural Netw.*, vol. 131, pp. 291–299, Nov. 2020.

[24] Y. Liu, S.-M. Shih, S.-L. Tian, Y.-J. Zhong, and L. Li, "Lower extremity joint torque predicted by using artificial neural network during vertical jump," *J. Biomechanics*, vol. 42, no. 7, pp. 906–911, May 2009.

[25] M. E. Hahn, "Feasibility of estimating isokinetic knee torque using a neural network model," *J. Biomechanics*, vol. 40, no. 5, pp. 1107–1114, Jan. 2007.

[26] M. H. Jali, T. A. Izzuddin, Z. H. Bohari, M. F. Sulaima, and H. Sarkawi, "Predicting EMG based elbow joint torque model using multiple input ANN neurons for arm rehabilitation," in *Proc. UKSim-AMSS 16th Int. Conf. Comput. Modeling Simulation*, Mar. 2014, pp. 189–194.

[27] B. Freriks and H. Hermens, "European recommendations for surface electromyography," *Roessingh Res. Develop.*, vol. 8, no. 2, pp. 13–54, 2000.

[28] M. P. Kadaba, H. K. Ramakrishnan, and M. E. Wootten, "Measurement of lower extremity kinematics during level walking," *J. Orthopaedic Res.*, vol. 8, no. 3, pp. 383–392, May 1990.

[29] R. B. Davis, S. Õunpuu, D. Tyburski, and J. R. Gage, "A gait analysis data collection and reduction technique," *Hum. Movement Sci.*, vol. 10, no. 5, pp. 575–587, Oct. 1991.

[30] C. Pizzolato, M. Reggiani, L. Modenese, and D. G. Lloyd, "Real-time inverse kinematics and inverse dynamics for lower limb applications using OpenSim," *Comput. Methods Biomech. Biomed. Eng.*, vol. 20, no. 4, pp. 436–445, Mar. 2017.

[31] M. Sartori, D. G. Llyod, and D. Farina, "Neural data-driven musculoskeletal modeling for personalized neurorehabilitation technologies," *IEEE Trans. Biomed. Eng.*, vol. 63, no. 5, pp. 879–893, May 2016.

[32] H. X. Hoang, C. Pizzolato, L. E. Diamond, and D. G. Lloyd, "Subject-specific calibration of neuromuscular parameters enables neuromusculoskeletal models to estimate physiologically plausible hip joint contact forces in healthy adults," *J. Biomechanics*, vol. 80, pp. 111–120, Oct. 2018.

[33] A. Mantoan, C. Pizzolato, M. Sartori, Z. Sawacha, C. Cobelli, and M. Reggiani, "MOtoNMS: A MATLAB toolbox to process motion data for neuromusculoskeletal modeling and simulation," *Source Code Biol. Med.*, vol. 10, no. 1, p. 12, Dec. 2015.

[34] T.-W. Lu and J. J. O'Connor, "Bone position estimation from skin marker co-ordinates using global optimisation with joint constraints," *J. Biomechanics*, vol. 32, no. 2, pp. 129–134, Feb. 1999.

[35] F. E. Zajac, R. R. Neptune, and S. A. Kautz, "Biomechanics and muscle coordination of human walking: Part I: Introduction to concepts, power transfer, dynamics and simulations," *Gait Posture*, vol. 16, no. 3, pp. 215–232, 2002.

[36] M. Sartori, M. Reggiani, D. G. Lloyd, and E. Pagello, "A neuromusculoskeletal model of the human lower limb: Towards EMG-driven actuation of multiple joints in powered orthoses," in *Proc. IEEE Int. Conf. Rehabil. Robot.*, Jun. 2011, pp. 1–6.

[37] D. G. Lloyd and T. F. Besier, "An EMG-driven musculoskeletal model to estimate muscle forces and knee joint moments *in vivo*," *J. Biomechanics*, vol. 36, no. 6, pp. 765–776, Jun. 2003.

[38] T. S. Buchanan, D. G. Lloyd, K. Manal, and T. F. Besier, "Neuromusculoskeletal modeling: Estimation of muscle forces and joint moments and movements from measurements of neural command," *J. Appl. Biomechanics*, vol. 20, no. 4, pp. 367–395, Nov. 2004.

[39] E. Ceseracciu *et al.*, "A flexible architecture to enhance wearable robots: Integration of EMG-informed models," in *Proc. IEEE/RSJ Int. Conf. Intell. Robots Syst. (IROS)*, Sep. 2015, pp. 4368–4374.

[40] X. Glorot, A. Bordes, and Y. Bengio, "Deep sparse rectifier neural networks," in *Proc. 14th Int. Conf. Artif. Intell. Statist.*, 2011, pp. 315–323.

[41] J. Schmidt-Hieber, "Nonparametric regression using deep neural networks with ReLU activation function," *Ann. Statist.*, vol. 48, no. 4, pp. 1875–1897, Aug. 2020.

[42] D. P. Kingma and J. Ba, "Adam: A method for stochastic optimization," 2014, *arXiv:1412.6980*. [Online]. Available: http://arxiv.org/abs/1412.6980

[43] S. Bock, J. Goppold, and M. Weiß, "An improvement of the convergence proof of the ADAM-optimizer," 2018, *arXiv:1804.10587*. [Online]. Available: http://arxiv.org/abs/1804.10587

[44] A. J. Meyer, C. Patten, and B. J. Fregly, "Lower extremity EMG-driven modeling of walking with automated adjustment of musculoskeletal geometry," *PLoS ONE*, vol. 12, no. 7, Jul. 2017, Art. no. e0179698.

[45] A. J. Thomas, M. Petridis, S. D. Walters, S. M. Gheytassi, and R. E. Morgan, "Two hidden layers are usually better than one," in *Proc. Int. Conf. Eng. Appl. Neural Netw.* Cham, Switzerland: Springer, 2017, pp. 279–290.

[46] C. Fan, F. Xiao, and Y. Zhao, "A short-term building cooling load prediction method using deep learning algorithms," *Appl. Energy*, vol. 195, pp. 222–233, Jun. 2017.

[47] F. Hug and S. Dorel, "Electromyographic analysis of pedaling: A review," *J. Electromyogr. Kinesiol.*, vol. 19, no. 2, pp. 182–198, Apr. 2009.

[48] J. M. Wakeling, O. M. Blake, and H. K. Chan, "Muscle coordination is key to the power output and mechanical efficiency of limb movements," *J. Experim. Biol.*, vol. 213, no. 3, pp. 487–492, Feb. 2010.

Longbin Zhang received the M.Sc. degree in control engineering from the South China University of Technology, Guangzhou, China, in 2017. She is currently pursuing the Ph.D. degree with a focus on robotic exoskeletons for patients with a motor disorder with the Department of Engineering Mechanics, KTH Royal Institute of Technology, Stockholm, Sweden.

She has participated in some research projects in Sweden sponsored by the Promobilia Foundation (ref. nr. 18200) and Swedish Scientific Council (2018-00750) and worked on biosignal processing and exoskeleton control. She has published several articles in international conferences and journals. Her main research interests include simulation of human movement, robotic exoskeleton assistive strategies, electromyography (EMG) control, and optimizing and reinforcement learning control.

Zhijun Li (Senior Member, IEEE) received the Ph.D. degree in mechatronics from Shanghai Jiao Tong University, Shanghai, China, in 2002.

From 2003 to 2005, he was a Post-Doctoral Fellow with the Department of Mechanical Engineering and Intelligent systems, The University of Electro-Communications, Tokyo, Japan. From 2005 to 2006, he was a Research Fellow with the Department of Electrical and Computer Engineering, National University of Singapore, Singapore, and Nanyang Technological University, Singapore. Since 2012, he has been a Professor with the College of Automation Science and Engineering, South China University of Technology, Guangzhou, China. Since 2017, he has been a Professor with the Department of Automation, University of Science and Technology, Hefei, China. His current research interests include service robotics, teleoperation systems, nonlinear control, and neural network optimization.

Dr. Li was the General Chair and the Program Chair of the 2016 and 2017 IEEE Conference on Advanced Robotics and Mechatronics. Since 2016, he has been the Co-Chair of the Technical Committee on Bio-mechatronics and Bio-robotics Systems (B^2S), the IEEE Systems, Man and Cybernetics Society, the Technical Committee on Neuro-Robotics Systems, and the IEEE Robotics and Automation Society. He has been serving as an Editor-at-Large of the *Journal of Intelligent and Robotic Systems* and an Associate Editor of several IEEE TRANSACTIONS.

Yingbai Hu received the M.Sc. degree in control theory and control engineering from the South China University of Technology, Guangzhou, China, in 2017. He is currently pursuing the Ph.D. degree in computer science with Technische Universität München, Munich, Germany.

He was a Research Fellow with the Shenzhen Institutes of Advanced Technology, Chinese Academy of Sciences, Beijing, China, from 2017 to 2018. He is also a member of the Informatics 6-Chair of Robotics, Artificial Intelligence and Real-time Systems, Technische Universität München. He has participated in the EU-funded project European Union's Horizon 2020 Framework Programme for Research and Innovation under the Specific Grant Agreement No. 785907 (Human Brain Project SGA2). He has published several articles in international conferences and journals. His main research interests include control and instrumentation in mobile robot, human–robot interaction, surgical robotics, and reinforcement learning.

Christian Smith (Member, IEEE) received the M.Sc. degree in engineering physics and the Ph.D. degree in computer science from the KTH Royal Institute of Technology, Stockholm, Sweden, in 2005 and 2009, respectively.

He was a Post-Doctoral Researcher with Advanced Telecommunications Research International (ATR), Kyoto, Japan, from 2010 to 2011. He is currently an Associate Professor of Computer Science and the Deputy Head of the Division of Robotics, Perception, and Learning, KTH Royal Institute of Technology. His research interests include control and modeling for manipulation and grasping in human-centric environments, such as medical facilities and small-scale manufacturing plants, as well as physical human–robot interaction.

Dr. Smith was the Treasury Chair of the IEEE International Conference on Robotics and Automation in 2016. He is also the Secretary of the IEEE Robotics and Automation Society Swedish Chapter. He also serves as an Associate Editor for the IEEE ROBOTICS AND AUTOMATION LETTERS and several conference editorial boards.

Elena M. Gutierrez Farewik received the B.Sc. degree in mechanical engineering from Cornell University, Ithaca, NY, USA, in 1995, the M.Sc. degree in biomedical engineering from the University of Michigan, Ann Arbor, MI, USA, in 1997, and the Ph.D. degree in orthopedics from Karolinska Institutet, Solna, Sweden, in 2003.

She is currently a Professor of Biomechanics with the Department of Engineering Mechanics, KTH Royal Institute of Technology, Stockholm, Sweden. She is also with the Department of Women's and Children's Health, Karolinska Institutet. She leads the research group at the KTH MoveAbility Lab. She and her group combine experiments with numerical modeling to study the short- and long-term consequences of deviating loading on musculoskeletal tissues in growing children. They are also developing biosignal-controlled assistive-as-needed devices for the lower extremities for applications in neurorehabilitation and rehabilitation, with a goal to preserve available neural pathways and complement the user's functional abilities. Her research interests span several biological scales and include modeling, predictive simulation, and device design for children and adults with motor disorders.

Ruoli Wang received the B.Eng. degree in mechanical engineering from Southeast University, Nanjing, China, in 2004, and the M.Sc. and Ph.D. degrees in engineering mechanics from the KTH Royal Institute of Technology, Stockholm, Sweden, in 2007 and 2012, respectively.

Her post-doctoral research at Paediatric Neurology Group, Karolinska Institutet, Stockholm, Sweden, and Computational Biology Group, KTH, centered around the quantification of spasticity and secondary muscle structure, and property changes following spasticity. At her current post as an Assistant Professor at KTH Engineering Sciences, Engineering Mechanics, her focus is to develop methodologies for estimating personalized musculotendon parameters noninvasively using a combination of medical imaging, musculoskeletal modeling, and optimization. She is also a member of the Research Group, KTH MoveAbility Lab, where she is also a member of the Executive Board of the KTH BioMEx Center. Her research interests include *in vivo* quantification of mechanical properties of the human muscle-tendon structure, neuromusculoskeletal modeling of human movement, and neurophysiology of human muscles.